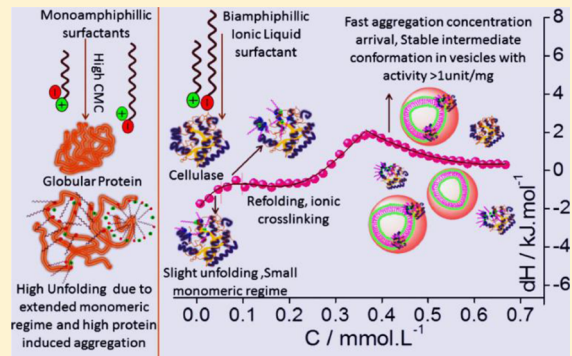


# Structural and Functional Stability of Cellulase in Aqueous-Biamphiphilic Ionic Liquid Surfactant Solution

Pankaj Bharmoria,<sup>†</sup> Mohit J. Mehta,<sup>‡</sup> Imran Pancha,<sup>†</sup> and Arvind Kumar<sup>\*,†,‡</sup><sup>†</sup>Academy of Scientific and Innovative Research (AcSIR) and <sup>‡</sup>Salt and Marine Chemical Discipline, Central Salt and Marine Chemicals Research Institute, Council of Scientific & Industrial Research (CSIR), G. B. Marg, Bhavnagar-364002, Gujarat, India**S Supporting Information**

**ABSTRACT:** In order to explore the potential of a biamphiphilic ionic liquid surfactant as an enzyme stabilizer in detergents, we have investigated the structural and functional stability of cellulase upon interaction with 3-methyl-1-octylimidazolium dodecylsulfate,  $[C_8\text{mim}][C_{12}\text{OSO}_3]$ , in aqueous medium at pH 4.8. Adsorption and binding isotherms determined from tensiometry and isothermal titration calorimetry indicated that  $[C_8\text{mim}][C_{12}\text{OSO}_3]$  interacts with cellulase distinctly at the three critical concentrations, viz., aggregation,  $C_1$ , saturation,  $C_2$ , and vesicular,  $C_3$ . Fluorescence (at  $\lambda_{\text{ex}} = 280$  nm), far UV-circular dichroism spectra, and dynamic light scattering results have shown that  $[C_8\text{mim}][C_{12}\text{OSO}_3]$  alters the tertiary and secondary structure of cellulase with a slight initial unfolding in the monomeric regime (up to  $C_1$ ), refolding in the aggregation regime (up to  $C_2$ ), and unfolding in the shared aggregation regimes (below  $C_3$ ) and stabilizes the altered conformation in the post-vesicular regime with an overall variation of hydrodynamic diameter from 4.12 to 7.19 nm. A dinitrosalicylic acid sugar assay test showed excellent functional stability of cellulase with an activity of  $\geq 1$  unit/mg in all the concentration regimes. A very good surface activity (*J. Phys. Chem. B* 2012, 116, 14363) complied by the present results vindicates the candidature of  $[C_8\text{mim}][C_{12}\text{OSO}_3]$  as a potential alternative of mixed micelles or nonionic surfactants for cellulase stabilization in detergent industries.



## 1. INTRODUCTION

Surface active ionic liquids (SAILS) is a class of ionic liquids (salts having melting point  $<100^\circ\text{C}$ ) which expands the liquid interface by getting adsorbed and forms self-assembled structures micelles/vesicles in the solution depending upon their amphiphilicity and structure of molecular ion. Although there is no hardliner difference in the literature, SAILS are differentiated from conventional ionic surfactants in terms of their low melting point ( $<100^\circ\text{C}$ ), usually superior surface activity, green nature (depending upon choice of cations/anions), and structural tunability. Tunability is one of the most significant properties of SAILS which has led to their emergence in the past decade from imidazolium cation based SAILS<sup>2–12,15–21</sup> to amino acid (aa) cations<sup>13,14</sup> and very recently to choline cation based SAILS with variable anions.<sup>22</sup> Biamphiphilic ionic liquid surfactants (BAILs) is one such example where amphiphilicity has been introduced in both the ionic moieties, leading to a significant improvement in surface activity and generation of a variety of self-assembled (micelles, aggregated micelles, or vesicles) structures.<sup>15</sup> Due to the superior accessible properties, SAILS can be potential future prospects for various surfactant based applications.

One of the most widespread applications of surfactants is their formulation with proteins in the field of pharmaceuticals, cosmetics, paints, coatings, detergents, and biochemical

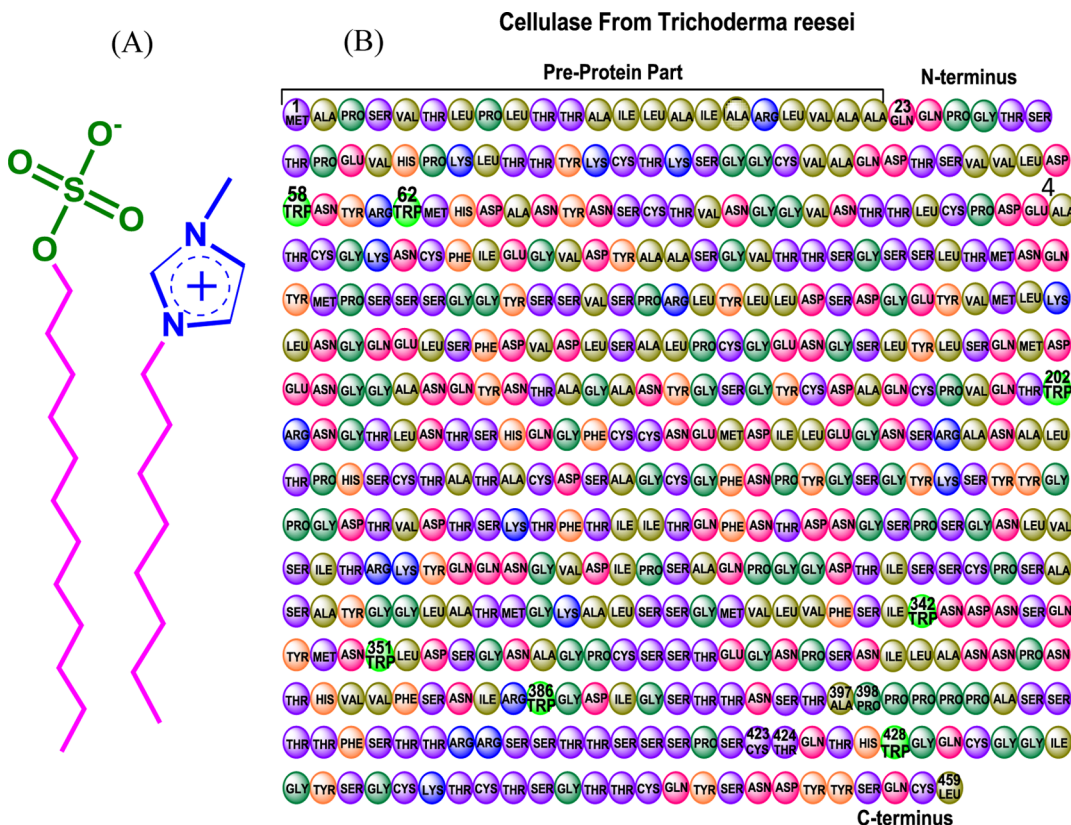
reactions.<sup>23–25</sup> Therefore, investigations on interactions of novel surfactants such as SAILS with proteins are indispensable for exploring their commercial applicability. There are only few reports where the effect of SAILS on the structure of proteins has been studied. These studies are limited mainly to bovine serum albumin (BSA) as a model protein.<sup>26,27,29–32,34</sup> 1-Tetradecyl-3-methylimidazolium bromide  $[C_{14}\text{mim}][\text{Br}]$  has been reported to protect the secondary structure but alter the tertiary structure of BSA below the cmc.<sup>26,27</sup> In earlier studies, we have also reported the effect of 3-methyl-1-octylimidazolium chloride  $[C_8\text{mim}][\text{Cl}]$  and 1-butyl-3-methylimidazolium octylsulfate  $[C_4\text{mim}][C_8\text{OSO}_3]$  on protein gelatin and BSA and 3-methyl-1-octylimidazolium dodecylsulfate  $[C_8\text{mim}][C_{12}\text{OSO}_3]$  on BSA using physical and spectroscopic techniques.<sup>28–30</sup> It was found that  $[C_8\text{mim}][\text{Cl}]$  is more effective in inducing changes in the structure of BSA compared to  $[C_4\text{mim}][C_8\text{OSO}_3]$  at low concentration, whereas both the SAILS denature the protein at higher concentration. On the other hand,  $[C_8\text{mim}][C_{12}\text{OSO}_3]$  induced refolding of BSA after initial unfolding at very low concentration and stabilized it against aggregation in the post-vesicular region.<sup>30</sup> Wang et al.

Received: June 23, 2014

Revised: July 22, 2014

Published: July 24, 2014

**Scheme 1.** (A) Chemical Structure of 3-Methyl-1-octylimidazolium Dodecylsulfate; (B) Amino Acid Sequencing of Enzyme, Cellulase Endo- $\beta$ -glucanase from *Trichoderma reesei*, E.C. Number 3.2.4.1<sup>a</sup>



<sup>a</sup>The structure has been redrawn from ref 36 with permission.

have studied the effect of ester-functionalized SAILs, 3-methyl-1-(ethoxycarbonylmethyl)imidazolium dodecylsulfate [ $C_1COOC_2C_1im][C_{12}OSO_3]$ ] and 3-methyl-1-(ethoxycarbonylmethyl)pyrrolidinium dodecylsulfate [ $C_1COOC_2C_1Py][C_{12}OSO_3]$ ], on the stability of BSA and reported that the imidazolium headgroup has a higher denaturation effect than that of pyrrolidinium.<sup>31</sup> Yan et al. have investigated the interaction of [ $C_nmim][Br]$  ( $n = 4, 6, 8, 10$ ) with BSA and concluded that [ $C_{10}mim][Br]$  induced marked changes in the secondary structure of BSA driven by strong hydrophobic interactions, whereas [ $C_nmim][Br]$  ( $n = 4, 6, 8$ ) induced marginal change in BSA secondary structure driven by hydrogen bonding and van der Waals interactions.<sup>32</sup> It has been shown that the pharmaceutical SAILs, cetylpyridinium salicylate and benzethonium salicylate, quench the fluorescence of human serum albumin and bind strongly to the hydrophobic sites.<sup>33</sup> Recently, Kumar et al. have reported from intrinsic time-resolved fluorescence decay and rotational-relaxation dynamics studies that 1-butyl-3-methylimidazolium tetrafluoroborate [ $C_4mim][BF_4]$ ] induced swelling of BSA rather than aggregation upon protein denaturation.<sup>34</sup>

The effect of SAILs on the structure of BSA as a model globular protein studied so far has a fundamental significance; however, considering the specific nature of different proteins,<sup>35</sup> it is necessary to get insights into their interactions with other globular proteins of practical significance. In this regard, we have investigated the effect of 3-methyl-1-octylimidazolium dodecylsulfate [ $C_8mim][C_{12}OSO_3]$ ], a biampiphilic ionic liquid (BAIL), on the structure and functionality of a laundry enzyme “cellulase” from *Trichoderma reesei* in aqueous media at

pH 4.8. Cellulase belongs to a class of hydrolytic enzymes which catalyze the hydrolysis of polysaccharide, cellulose, and its other oligosaccharide derivatives. Cellulase from *Trichoderma reesei* used in the present study is an endo- $\beta$ -glucanase having enzyme commission number 3.2.14. It is a 48 kDa globular protein with 459 aa residues in its primary structure.<sup>36</sup> The structure of cellulase is composed of a catalytic domain (CD) between aa number 23 and 397 and cellulose binding domain (CBD) from aa 424 to 459 which are linked by linker sequences from aa 398 to 423.<sup>37</sup> Cellulases have earlier been investigated for their interaction with conventional surfactants.<sup>38–40</sup> From ITC, fluorescence, and CD spectral investigations, Xiang et al. have reported that sodium dodecyl sulfate (SDS) micelles exert a dual effect on cellulase by binding both as a denaturant and as a recovery reagent.<sup>38</sup> They reported that SDS denatured the cellulase up to 45 mM with a loss in enzyme activity, followed by a recovery of  $\alpha$ -helical structure and a 1.3-fold rise in enzyme activity between 75 and 100 mM due to hydrophobic stabilization of enzymes by SDS micelles. Rastegari et al. have reported a biphasic fluorescence quenching mechanism of cellulase from *Aspergillus niger* by cationic surfactants, *n*-alkyl trimethylammonium bromides ( $C_nTAB$ ,  $n = 12$  and 14) showing two types of binding sites (electrostatic and hydrophobic) on cellulase.<sup>39</sup> Eriksen et al. have investigated the effect of various nonionic, cationic, and anionic surfactants on cellulase of *Trichoderma reesei*, and found that nonionic surfactant along with anionic surfactant reduces the Cel7A adsorption on lignocellulose due to higher hydrophobic interaction of lignocellulose with surfactant leading to an increase in enzymatic hydrolysis.<sup>40</sup> Motivation of the present

work is based on the hypothesis that reduction in aggregation concentration of surfactant lessens the number of surfactant monomers interacting with enzymes, thus reducing the denaturation effect.<sup>30,41,42</sup> Cationic vesicles formed by nonstoichiometric mixing of cationic and anionic surfactants are other such systems which have also been studied for their binding with globular proteins.<sup>43,44</sup>  $[C_8\text{mim}][C_{12}\text{OSO}_3]$  used in the present study has a critical aggregation concentration (CAC) of 0.35 mmol L<sup>-1</sup> which is very low compared to its individual constituents as a surfactants, i.e.,  $[C_8\text{mim}][\text{Cl}]$  ( $\sim$ 108 mmol L<sup>-1</sup>)<sup>45</sup> and SDS ( $\sim$ 8 mmol L<sup>-1</sup>). Also,  $[C_8\text{mim}][C_{12}\text{OSO}_3]$  is expected to stabilize the structure and functionality of cellulase considering the fact that  $[C_8\text{mim}][C_{12}\text{OSO}_3]$  ions will have a higher affinity for each other than for the cellulase surfactant system.

In this work, various concentration regimes of  $[C_8\text{mim}][C_{12}\text{OSO}_3]$  interaction with cellulase have been defined by adsorption isotherms using tensiometry and binding isotherms using isothermal titration calorimetry. The enthalpy changes due to binding of  $[C_8\text{mim}][C_{12}\text{OSO}_3]$  ions to cellulase have been determined from the binding isotherm. Structural (tertiary and secondary) alterations in cellulase due to  $[C_8\text{mim}][C_{12}\text{OSO}_3]$  binding have been demonstrated through fluorescence and circular dichroism spectroscopic techniques. Dynamic light scattering has been used to validate the structural alterations observed from fluorescence and CD spectral results. Functional activity of cellulase in different concentration regimes of  $[C_8\text{mim}][C_{12}\text{OSO}_3]$ –cellulase interaction was detected through a dinitrosalicylic acid sugar assay test using carboxymethyl cellulose as the substrate.

## 2. EXPERIMENTAL SECTION

**2.1. Materials.** 1-Bromooctane with purity >98% and cellulase from *Trichoderma reesei* ATCC26921 (lyophilized powder,  $\geq$ 1 unit/mg) were purchased from Sigma-Aldrich. 1-Methylimidazole of AR grade was purchased from Spectrochem, India. Sodium dodecyl sulfate (SDS) >95% was purchased from TCI (Chemical), India. Ethyl acetate and dichloromethane of AR grade were procured from s d fine-chem Ltd., India. 3-Methyl-1-octylimidazolium dodecylsulfate,  $[C_8\text{mim}][C_{12}\text{OSO}_3]$ , was synthesized using the procedure reported in one of our earlier publications.<sup>15</sup> The solutions (w/v) of  $[C_8\text{mim}][C_{12}\text{OSO}_3]$  with or without cellulase were prepared using an analytical balance with a precision of  $\pm 0.0001$  g (Denver Instrument APX-200) in acetate buffer (50 mM, pH 4.8). The buffer solution was prepared in degassed Millipore grade water using AR-grade sodium acetate (99%) and acetic acid (99.7%) purchased from SRL, India. The concentration of cellulase used in buffer solution is 0.1%. The stock solution of cellulase was stored at 4 °C. The molecular structure of  $[C_8\text{mim}][C_{12}\text{OSO}_3]$  and aa sequences of cellulase are depicted in Scheme 1.

**2.2. Methods.** **2.2.1. Tensiometry.** Tensiometry has been used to calculate the aggregation concentration of  $[C_8\text{mim}][C_{12}\text{OSO}_3]$  in buffer and to define the concentration regimes of  $[C_8\text{mim}][C_{12}\text{OSO}_3]$  interaction with 0.1% cellulase from adsorption isotherms. The technique also gives indirect information about the relative surface excess of surface active species ( $\Gamma_{\max}$ ) at the interface via the Gibbs adsorption equation (eq 1, Supporting Information). Surface tension measurements were carried out at 298.15 K using a Data Physics DCAT II automated tensiometer employing the Wilhelmy plate method. A concentrated solution of  $[C_8\text{mim}]$

$[C_{12}\text{OSO}_3]$  (10 times above the critical aggregation concentration) was added by volume into the base solution, stirred for 3 min, and equilibrated for 5 min before measurement. The data was collected in triplicate, and the error in surface tension measurements was found to be  $\pm 0.1$  mN·m<sup>-1</sup>.

**2.2.2. Isothermal Titration Calorimetry.** Enthalpy changes (dH) due to interaction of  $[C_8\text{mim}][C_{12}\text{OSO}_3]$  with cellulase in buffer solution were measured using a MicroCal ITC200 microcalorimeter, with an instrument controlled Hamiltonian syringe having a volume capacity of 40 μL. The titration was done by adding 1 μL aliquots of  $[C_8\text{mim}][C_{12}\text{OSO}_3]$  stock solution into the sample cell containing 200 μL of acetate buffer or 0.1% cellulase solution with continuous stirring at 500 rpm. The parameters like time of addition and duration between each addition were controlled by software provided with the instrument. The dH at each injection was measured and plotted against concentration by using origin software provided with the instrument. The  $[C_8\text{mim}][C_{12}\text{OSO}_3]$ –cellulase binding isotherm was used to define various concentration regimes.

**2.2.3. Fluorimetry.** Alterations in the tertiary structure of cellulase upon interaction with  $[C_8\text{mim}][C_{12}\text{OSO}_3]$  were analyzed through a Fluorolog (Horiba Jobin Yvon) spectrometer using a quartz cuvette of path length 1 cm. Changes in the intrinsic fluorescence of cellulase were analyzed at an excitation/emission wavelength ( $\lambda_{\text{ex}}/\lambda_{\text{em}}$ ) of 280/340 nm (slit width = 1 nm) in a quartz cuvette of 1 cm path length. The maximal values of fluorescence are the average of three measurements. The fluorescence spectra were corrected for the instrumental response.

**2.2.4. Far-UV Circular Dichroism Spectroscopy.** Alterations in the secondary structure ( $\beta$ -sheet) of cellulase upon interaction with  $[C_8\text{mim}][C_{12}\text{OSO}_3]$  were monitored through a Jasco J-815 CD spectrometer at 298.15 K in the far UV region ( $\lambda = 200$ –250 nm). Spectra were collected in a 1 mm path length quartz cuvette at a scan rate of 50 nm/min and sensitivity of 100 mdeg. The response time and the bandwidth were 2 s and 0.2 nm, respectively.

**2.2.5. Dynamic Light Scattering.** Changes in the size of native cellulase upon interaction with  $[C_8\text{mim}][C_{12}\text{OSO}_3]$  were monitored at 298.15 K, using a NaBiTec Spectro Size 300 light scattering apparatus (Germany) with a He–Ne laser (633 nm, 4 Mw). The hydrodynamic measurements were carried out in a quartz cuvette of 1 cm path length by preparing separate  $[C_8\text{mim}][C_{12}\text{OSO}_3]$ –cellulase solutions of desired concentrations and measuring their viscosities and refractive indices. The data evaluation of the dynamic light scattering measurements was performed with the built-in CONTIN algorithm. The error observed in the size of cellulase was  $\pm 0.2$  nm, and that in the size of the vesicle was  $\pm 5$  nm.

**2.2.6. Functional Stability of Cellulase.** Functional stability of cellulase at different concentrations (0, 0.004, 0.022, 0.071, 0.37, 0.7, and 4.0 mmol L<sup>-1</sup>) of  $[C_8\text{mim}][C_{12}\text{OSO}_3]$  was detected through a dinitrosalicylic acid (DNS) sugar assay test using carboxymethyl cellulose (CMC) as the substrate. First of all, a standard calibration curve (sugar concentration vs absorbance) was prepared using DNS analysis. 1% cellulase (100 μL) + 1% CMC (900 μL) solutions at different concentrations of  $[C_8\text{mim}][C_{12}\text{OSO}_3]$  were incubated for 20 min at 45 °C. The reaction was stopped by adding 1 mL of DNS reagent. The solutions were then heated at 90 °C on a boiling water bath for 15 min until the appearance of a deep red color due to reduction of the nitro group of DNS to the amino group by sugar produced during hydrolysis of CMC. There-

after, 0.33 mL of a 40% solution of Rochelle salt was added to stabilize the color. Solutions were cooled in a cold water bath diluted up to 10 mL, and absorbance was measured at 546 nm. The measured absorbance was matched with a standard calibration curve to calculate the sugar concentration. Enzyme activity was calculated using the standard equation (Annexure 1, Supporting Information).

### 3. RESULTS AND DISCUSSION

#### 3.1. Defining the Concentration Regimes of $[C_8\text{mim}][C_{12}\text{OSO}_3]$ –Cellulase Interaction. 3.1.1. Adsorption Isotherm.

Figure 1 shows the comparison of adsorption isotherms

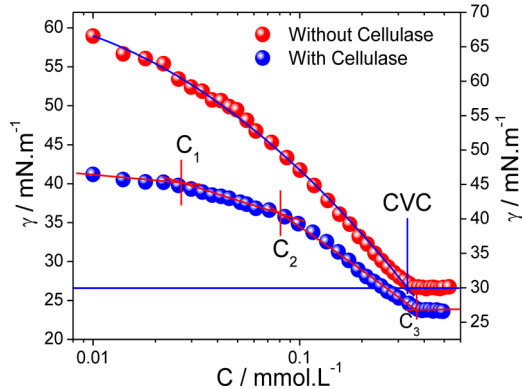


**Figure 1.** Adsorption isotherms of  $[C_8\text{mim}][C_{12}\text{OSO}_3]$  in buffer and cellulase solution. Various transitions discussed in the text are marked with vertical lines.

of  $[C_8\text{mim}][C_{12}\text{OSO}_3]$  in buffer and in 0.1% cellulase solution. The surface tension ( $\gamma$ ) of buffer decreased polynomially with the addition of  $[C_8\text{mim}][C_{12}\text{OSO}_3]$  and attained constancy at  $0.35 \text{ mmol L}^{-1}$  (critical vesicular concentration, CVC), due to the saturation of the interface, whereas three definite transitions, defined as the critical aggregation concentration  $C_1$  (CAC), the saturation concentration  $C_2$  (SC), and the critical vesicular concentration  $C_3$  (CVC), were observed in the  $[C_8\text{mim}][C_{12}\text{OSO}_3]$ –cellulase adsorption isotherm. The result is different from that of the  $[C_8\text{mim}][C_{12}\text{OSO}_3]$ –BSA adsorption isotherm<sup>35</sup> where only CAC and CVC were observed, thus signifying the specificity of two different globular proteins toward  $[C_8\text{mim}][C_{12}\text{OSO}_3]$ . The  $\gamma$  of cellulase solution decreased from  $49.73$  to  $44.84 \text{ mN}\cdot\text{m}^{-1}$  up to  $C_1$  ( $0.026 \text{ mmol L}^{-1}$ ) due to adsorption of surface active  $[C_8\text{mim}][C_{12}\text{OSO}_3]$ –cellulase (monomer complexes) at the interface. Above  $C_1$ ,  $[C_8\text{mim}][C_{12}\text{OSO}_3]$  aggregated on the cellulase surface by the cooperative effect of electrostatic and hydrophobic interaction, thus forming  $[C_8\text{mim}][C_{12}\text{OSO}_3]$ –

cellulase (aggregate complexes), causing a decrease in  $\gamma$  to  $40.88 \text{ mN}\cdot\text{m}^{-1}$  at  $C_2$  ( $0.08 \text{ mmol L}^{-1}$ ). After  $C_2$ , the  $\gamma$  decreased sharply due to the adsorption of  $[C_8\text{mim}][C_{12}\text{OSO}_3]$  monomers at the interface, since cellulase gets saturated with  $[C_8\text{mim}][C_{12}\text{OSO}_3]$  up to  $C_2$ . The  $\gamma$  decreased to  $26.69 \text{ mN}\cdot\text{m}^{-1}$  until  $C_3$  ( $0.39 \text{ mmol L}^{-1}$ ) and attained constancy thereafter, thus signifying the interfacial saturation and beginning of vesicle formation. A small difference of  $0.04 \text{ mmol L}^{-1}$  in the CVC in the presence and absence of cellulase indicates that not many  $[C_8\text{mim}][C_{12}\text{OSO}_3]$  ions bind to cellulase. Various surface and bulk thermodynamic parameters such as maximum surface excess concentration ( $\Gamma_{\max}$ ), area of exclusion per monomer ( $A_{\min}$ ), Gibbs free energy of interfacial adsorption ( $\Delta G_{\text{ad}}^{\circ}$ ), Gibbs free energy of aggregation ( $\Delta G_{\text{agg}}^{\circ}$ ), standard enthalpy of aggregation ( $\Delta H_{\text{agg}}^{\circ}$  from ITC), and standard entropy of aggregation ( $\Delta S_{\text{agg}}^{\circ}$ ) of  $[C_8\text{mim}][C_{12}\text{OSO}_3]$  in buffer and in  $0.1\%$  cellulase solution are calculated using relevant equations (see Annexure 1, Supporting Information) and are given in Table 1.  $\Gamma_{\max}$  is lower and  $A_{\min}$  is higher for the  $[C_8\text{mim}][C_{12}\text{OSO}_3]$ –cellulase system, indicating that a lesser amount of surfactant is adsorbed at the interface in the presence of cellulase which is due to weak interaction between  $[C_8\text{mim}][C_{12}\text{OSO}_3]$  and cellulase which is also supported by a lower value of  $\Delta G_{\text{ad}}^{\circ}$  ( $-31.31 \text{ kJ mol}^{-1}$ ) observed in the presence of cellulase. Comparing the  $\Delta H_{\text{agg}}^{\circ}$  and  $\Delta S_{\text{agg}}^{\circ}$  values both in buffer and  $0.1\%$  cellulase, it has been found that the  $[C_8\text{mim}][C_{12}\text{OSO}_3]$  aggregation is entropy driven. The feasibility of  $[C_8\text{mim}][C_{12}\text{OSO}_3]$ –cellulase interaction has also been calculated using eq 1.<sup>46</sup>

$$\Delta G_{\text{PS}}^{\circ} = \Delta G_b^{\circ} - \Delta G_{\text{CVC}}^{\circ} = -RT \ln \frac{X_{\text{CAC}}}{X_{\text{CVC}}} \quad (1)$$

where  $\Delta G_{\text{PS}}^{\circ}$  is the standard free energy of polymer–surfactant interaction,  $\Delta G_b^{\circ}$  is the standard free energy of surfactant aggregation on polymer,  $\Delta G_{\text{CVC}}^{\circ}$  is the standard free energy of aggregation of surfactant in polymer solution,  $R$  is the universal gas constant,  $T$  is the temperature in Kelvin, and  $X_{\text{CAC}}$  and  $X_{\text{CVC}}$  are the mole fractions of  $[C_8\text{mim}][C_{12}\text{OSO}_3]$  at CAC and CVC in  $0.1\%$  cellulase solution. A low calculated value of  $\Delta G_{\text{PS}}^{\circ} = -6.7 \text{ kJ mol}^{-1}$  indicates a lower feasibility of  $[C_8\text{mim}][C_{12}\text{OSO}_3]$  interaction with cellulase, thus supporting the present context of hypothesis that  $[C_8\text{mim}][C_{12}\text{OSO}_3]$  ions have more interaction for each other than for cellulase in the solution.

3.1.2. Binding Isotherm. The thermograms of  $[C_8\text{mim}][C_{12}\text{OSO}_3]$  aggregation in buffer, cellulase solution and binding to cellulase at  $298.15 \text{ K}$  are shown in Figure 2. Inset of Figure 2 shows the dP plot of  $[C_8\text{mim}][C_{12}\text{OSO}_3]$  binding to cellulase. The aggregation of  $[C_8\text{mim}][C_{12}\text{OSO}_3]$  in buffer is mostly

**Table 1.** Thermodynamic Parameters Obtained from Surface Tension (ST) and Isothermal Titration Calorimetry (ITC) Techniques at  $298.15 \text{ K}^a$

sample	parameter							
	CVC (mmol L <sup>-1</sup> )		$\Gamma_{\max} \times 10^6$	$A_{\min}$	$\Delta G_{\text{agg}}^{\circ}$	$\Delta G_{\text{ad}}^{\circ}$	$\Delta H_{\text{agg}}^{\circ}$	$\Delta S_{\text{agg}}^{\circ}$
ST	ITC							
$[C_8\text{mim}][C_{12}\text{OSO}_3]$ + buffer	0.35	0.31	6.89	0.24	-25.63	-32.20	-9.36	54.56
$[C_8\text{mim}][C_{12}\text{OSO}_3]$ + 0.1% cellulase	0.39	0.35	3.93	0.42	-25.55	-31.31	-8.37	57.62

<sup>a</sup>The Gibbs surface excess ( $\Gamma_{\max}$ ), area of exclusion per monomer ( $A_{\min}$ ), standard free energy of aggregation ( $\Delta G_{\text{agg}}^{\circ}$ ), standard free energy of adsorption ( $\Delta G_{\text{ad}}^{\circ}$ ), and standard enthalpy of aggregation ( $\Delta H_{\text{agg}}^{\circ}$ ) at  $298.15 \text{ K}$  are expressed in  $\text{mol}\cdot\text{m}^{-2}$ ,  $\text{nm}^2\cdot\text{molecule}^{-1}$ , and  $\text{kJ mol}^{-1}$ , and the standard entropy of aggregation ( $\Delta S_{\text{agg}}^{\circ}$ ) is expressed in  $\text{J}\cdot\text{K}^{-1}\cdot\text{mol}^{-1}$ .

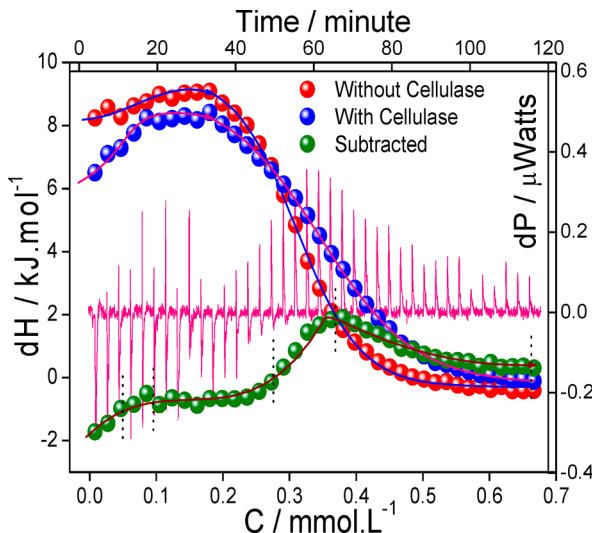


**Figure 2.** ITC thermograms of  $[C_8\text{mim}][C_{12}\text{OSO}_3]$  aggregation in buffer, cellulase solution and binding isotherm with cellulase. Inset shows the differential power ( $dP$ ) plot of  $[C_8\text{mim}][C_{12}\text{OSO}_3]$  binding with cellulase at sequential injection. Lines marking different concentration regimes of  $[C_8\text{mim}][C_{12}\text{OSO}_3]$ -cellulase interaction are discussed in the text.

endothermic and switched to exothermic post CVC (at  $0.50 \text{ mmol L}^{-1}$ ). The exothermic heat changes post CVC are due to inter-vesicular interactions. The standard enthalpy ( $\Delta H_{\text{agg}}^\circ$ ) of  $[C_8\text{mim}][C_{12}\text{OSO}_3]$  aggregation in buffer and cellulase solution was calculated by subtracting the heat changes in post and pre CVC region as shown in Figure S1, Supporting Information. The  $\Delta H_{\text{agg}}^\circ$  in buffer and cellulase solution was found to be  $-9.36$  and  $-8.37 \text{ kJ mol}^{-1}$ , respectively. The actual binding isotherm of  $[C_8\text{mim}][C_{12}\text{OSO}_3]$  to cellulase was obtained by subtracting the  $[C_8\text{mim}][C_{12}\text{OSO}_3]$  aggregation isotherm in buffer from the  $[C_8\text{mim}][C_{12}\text{OSO}_3]$ -cellulase binding isotherm in buffer. The binding isotherm of  $[C_8\text{mim}][C_{12}\text{OSO}_3]$  to cellulase has been divided into monomeric ( $0$ – $0.027 \text{ mmol L}^{-1}$ ), aggregation ( $0.027$ – $0.085 \text{ mmol L}^{-1}$ ), shared aggregation ( $0.085$ – $0.27 \text{ mmol L}^{-1}$ ), vesicular ( $0.27$ – $0.31 \text{ mmol L}^{-1}$ ), and post-vesicular ( $\geq 0.31 \text{ mmol L}^{-1}$ ) regimes. In conventional surfactant–protein systems, the exothermic and endothermic enthalpy changes signify the electrostatically driven binding and binding coupled with protein unfolding due to predominant hydrophobic interactions.<sup>35,47</sup>  $[C_8\text{mim}][C_{12}\text{OSO}_3]$  binds to cellulase in a sigmoidal fashion until  $C_3$  (CVC), which is indicative of sequential binding (electrostatic followed by hydrophobic interaction). This behavior is due to the presence of both ionic and hydrophobic sites on cellulase, owing to the presence of differentially polar aa. The binding is exothermic in the pre-vesicular regime and switched to endothermic thereafter. The exothermic binding in the pre-vesicular regime ( $\text{IL}/\text{cellulase} = 31.2 \text{ mol}$ ) indicates the predominance of electrostatic interactions over hydrophobic interactions. The change in slope of the curve at  $C_2$  (SC) indicates the beginning of shared aggregates interaction with cellulase by cooperative electrostatic and hydrophobic interactions. The  $dH$  released due to binding of  $2.76 \text{ mol}$  of  $[C_8\text{mim}][C_{12}\text{OSO}_3]$  to cellulase at  $C_1$  and  $8.62 \text{ mol}$  at  $C_2$  are  $-1.46$  and  $-0.51 \text{ kJ mol}^{-1}$ , respectively, which indicates the predominant electrostatic binding until  $C_1$ . The interaction of  $[C_8\text{mim}][C_{12}\text{OSO}_3]$  vesicles with cellulase in the vesicular and post-vesicular regime is entirely endothermic, which signifies

the predominance of hydrophobic interactions. This is due to the residence of cellulase in the hydrophobic bilayer of the vesicles which is also supported from an increase in size of vesicles in the post-vesicular regimes determined from DLS measurements. The  $dH$  absorbed due to interaction of vesicles with cellulase at  $C_3$ , CVC ( $\text{IL}/\text{cellulase} = 45.6 \text{ mol}$ ), is  $1.84 \text{ kJ mol}^{-1}$ . The CAC of  $[C_8\text{mim}][C_{12}\text{OSO}_3]$  is attained at very low concentration ( $0.026 \text{ mmol L}^{-1}$ ) in cellulase compared to BSA ( $0.11 \text{ mmol L}^{-1}$ )<sup>30</sup> owing to the lesser number of cationic and anionic aa in cellulase ( $57$ )<sup>36</sup> compared to BSA ( $197$ )<sup>48</sup> and different folding pattern, thus reducing the number of ionic sites for electrostatic binding in cellulase. In order to understand the site specific binding of the individual ion of  $[C_8\text{mim}][C_{12}\text{OSO}_3]$  in the monomeric regime of the  $[C_8\text{mim}][C_{12}\text{OSO}_3]$ –cellulase system, we measured the heat changes of SDS (Figure S2A and B, Supporting Information) and  $[C_8\text{mim}][\text{Cl}]$  (Figure S2C and D, Supporting Information) binding to cellulase up to  $0.14 \text{ mmol L}^{-1}$ . Exothermic enthalpy changes until around  $0.05 \text{ mmol L}^{-1}$  in both of the systems vindicate the predominance of site specific electrostatic interactions with oppositely charged aa residues in cellulase. The  $dH$  released in the case of the  $[C_8\text{mim}][\text{Cl}]$ –cellulase system ( $0.9 \text{ kJ mol}^{-1}$ ) is higher than that of the SDS–cellulase system ( $0.42 \text{ kJ mol}^{-1}$ ), indicating the dominance of negatively charged residues at the surface of cellulase. Also, the combined  $dH$  of both of the systems ( $-1.32 \text{ kJ mol}^{-1}$ ) at  $0.027 \text{ mmol L}^{-1}$  is comparable to  $-1.45 \text{ kJ mol}^{-1}$  released at the same concentration of  $[C_8\text{mim}][C_{12}\text{OSO}_3]$  upon cellulase binding. The reported ITC study of the SDS–cellulase<sup>38</sup> system also shows exothermic heat changes at low concentration, thus supporting the present results.

**3.2. Structural Alterations in Cellulase upon  $[C_8\text{mim}][C_{12}\text{OSO}_3]$  Binding.** **3.2.1. Alterations in the Tertiary Structure.** Changes in the intrinsic fluorescence at an excitation ( $\lambda_{\text{ex}}$ )/emission ( $\lambda_{\text{em}}$ ) wavelength of  $280 \text{ nm}/340 \text{ nm}$  have been used as a tool to reveal the changes in the tertiary structure of cellulase upon  $[C_8\text{mim}][C_{12}\text{OSO}_3]$  binding.<sup>35,49</sup> Shift in emission wavelength ( $\Delta\lambda_{\text{em}}$ ) of protein and variation in fluorescence intensity ( $I_{\text{flr}}$ ) are indicative of change in microenvironment of fluorophore and folding alteration. Cellulase absorbs ultraviolet light around  $280$  and  $230 \text{ nm}$  (Figure S3, Supporting Information) due to  $n-\pi^*$  transitions of aromatic aa residues and  $\pi-\pi^*$  transitions in the protein backbone. Negligible absorption and emission of pure  $[C_8\text{mim}][C_{12}\text{OSO}_3]$  compared to cellulase (Figures S3 and S4, Supporting Information) in the concerned concentration regimes discounts the possibility of an inner filter effect due to  $[C_8\text{mim}][C_{12}\text{OSO}_3]$ . The fluorescence emission spectra of the  $[C_8\text{mim}][C_{12}\text{OSO}_3]$ –cellulase system at  $\lambda_{\text{ex}}$  of  $280 \text{ nm}$  is shown in Figure 3, and the corresponding  $\lambda_{\text{em}}$  vs  $[C_8\text{mim}][C_{12}\text{OSO}_3]$  concentration profile is shown in Figure S6 (Supporting Information).

Fluorescence emission of cellulase at  $\lambda_{\text{ex}}$  of  $280 \text{ nm}$  arises from the aromatic aa residues like tryptophan (Trp), phenylalanine (Phe), and tyrosine (Tyr). Cellulase has 39 fluorescent aa (7 Trp, 22 Tyr, and 10 Phe) in different domains (Scheme 1). Owing to its low quantum yield, the contribution of Phe in the fluorescence of proteins is usually ignored. Thus, the fluorescence of cellulase is expected to be contributed mainly by 7 Trp and 22 Tyr residues. The decrease or increase in fluorescent intensity ( $I_{\text{flr}}$ ) of cellulase indicates the change in microenvironment of these residues due to structural alterations.  $I_{\text{flr}}$  did not change much with the addition of

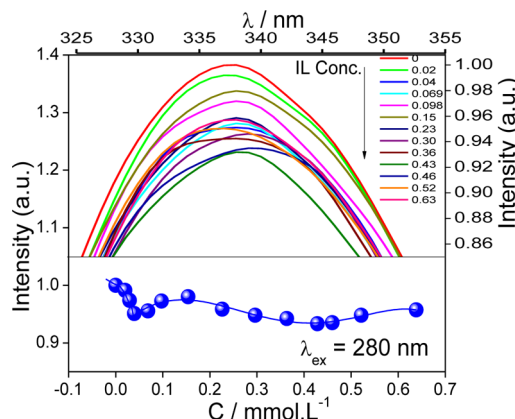


**Figure 3.** Fluorescence emission spectra and corresponding intensity variation of cellulase at different concentrations of  $[C_8\text{mim}][C_{12}\text{OSO}_3]$  at  $\lambda_{\text{ex}} = 280$  nm.

$[C_8\text{mim}][C_{12}\text{OSO}_3]$ , as 6.6% has been the maximum decrease in intensity observed in the vesicular regime. Only a 4.2% initial decrease in  $I_{\text{flr}}$  was observed until  $0.04 \text{ mmol L}^{-1}$  (just above  $C_1$ ), due to electrostatically induced unfolding of cellulase by site specific binding of  $[C_8\text{mim}][C_{12}\text{OSO}_3]$  ions to charged aa residues on the surface of protein. It has been confirmed from the recorded fluorescence spectra of  $[C_8\text{mim}][\text{Cl}]$ –cellulase (Figure S6A and B, Supporting Information) and SDS–cellulase (Figure S7A and B, Supporting Information) systems in the monomeric regime that  $[C_8\text{mim}]$  is the major contributor to the cellulase unfolding. The  $I_{\text{flr}}$  decreased until  $0.04 \text{ mmol L}^{-1}$  and increased thereafter in the  $[C_8\text{mim}][\text{Cl}]$ –cellulase system, whereas it increased all the way in the SDS–cellulase system. The higher  $dH$  released in the  $[C_8\text{mim}][\text{Cl}]$ –cellulase binding isotherm compared to the SDS–cellulase binding isotherm (discussed earlier) in this regime also confirms the fact that  $[C_8\text{mim}]^+$ –cellulase electrostatic interactions are more feasible which are due to a higher concentration of negatively charged aspartic (Asp) and glutamic acid (Glu) residues on the surface of cellulase. Above  $0.04 \text{ mmol L}^{-1}$ , the  $I_{\text{flr}}$  increased by 3% until  $0.15 \text{ mmol L}^{-1}$  due to refolding of cellulase, driven by cross-linking of  $[C_8\text{mim}][C_{12}\text{OSO}_3]$  with the charged and hydrophobic sites of cellulase in the aggregation regime.<sup>30,41,50</sup> The  $I_{\text{flr}}$  decreased again from the shared aggregation to the vesicular regime by 4.46%. The shared aggregation region is known as the region of maximum destabilization of protein in surfactant–protein chemistry due to the increased level of hydrophobic interactions between the surfactant aggregates of different protein molecules.<sup>35</sup> In the post-vesicular regime,  $I_{\text{flr}}$  increased slightly and remained almost constant thereafter, thus indicating the stabilization of cellulase in  $[C_8\text{mim}][C_{12}\text{OSO}_3]$  vesicles. No significant  $\Delta\lambda_{\text{em}}$  was observed (Figure S5, Supporting Information) in all of the concentration regimes, thus citing the fact that either the fluorescent residues (Trp, Tyr) are present in the interior of the cellulase or  $[C_8\text{mim}][C_{12}\text{OSO}_3]$  does not bind in their vicinity.

**3.2.2. Alterations in the Secondary Structure.** Far-UV CD spectra of proteins reveal the alterations in their secondary structure ( $\alpha$ -helical,  $\beta$ -sheet, turn) due to unfolding/refolding upon surfactant binding, and can also validate the complementary alterations in the tertiary structure.<sup>35,51</sup>  $\beta$ -sheet and turn structures predominate the N- and C-terminal regions of the cellulase with scarce distribution of  $\alpha$ -helices, whereas the middle parts are mainly dominated by  $\beta$ -sheets along with  $\alpha$ -

helices.<sup>36,37</sup> Thus, the  $\beta$ -sheet has the major contribution to the secondary structure of cellulase. The CD spectrum of native cellulase and at different concentrations of  $[C_8\text{mim}][C_{12}\text{OSO}_3]$  is shown in Figure 4. The peak at  $-\theta_{217 \text{ nm}}$  in cellulase is

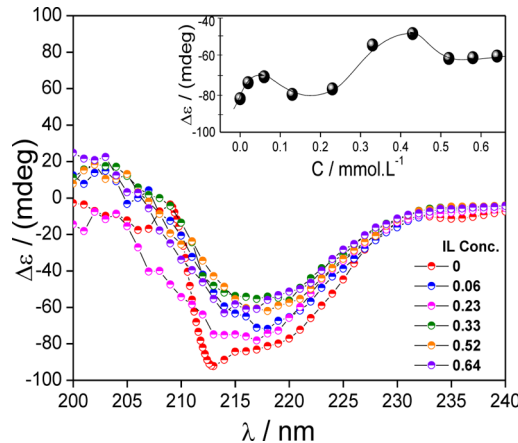


**Figure 4.** Far-UV CD spectra of cellulase as a function of  $[C_8\text{mim}][C_{12}\text{OSO}_3]$  concentration. The inset shows variation of the  $-\theta_{217 \text{ nm}}$  peak.

indicative of  $\beta$ -sheet structure. The inset in Figure 4 shows qualitative variation in the  $\beta$ -sheet structure as a function of  $[C_8\text{mim}][C_{12}\text{OSO}_3]$  concentration. Qualitatively continuous unfolding–refolding of cellulase has been observed from the secondary structural analysis which is complementary to that observed in fluorescence results. The  $\beta$ -sheet structure of cellulase decreased initially by 11% in the monomeric regime followed by a gain of 9% in the aggregation region. Then, there is a decrease of 31% from the sub-aggregation to vesicular regime followed by a gain of 13% in the post-vesicular regime. The  $\beta$ -sheet structure remained constant in the post-vesicular regime. Quantitative changes in  $\beta$ -sheet content were calculated from the instrument built-in secondary structure analysis software and are shown in Figure S8 (Supporting Information) and Table 2. Native cellulase has 57%  $\beta$ -sheet content, which is

**Table 2. Variation in the  $\beta$ -Sheet Content of Cellulase as a Function of  $[C_8\text{mim}][C_{12}\text{OSO}_3]$  Concentration**

$[C_8\text{mim}][C_{12}\text{OSO}_3]$ conc. (mmol L <sup>-1</sup> )	$\beta$ -sheet (%)
0	57.5
0.019	47.1
0.039	40.9
0.059	38.9
0.097	40.2
0.13	46.9
0.23	46.0
0.38	46.2
0.47	49.2
0.58	48.2

corroborates with the report of Penttilä that cellulase has maximum contribution from the  $\beta$ -sheet content.<sup>36</sup> The observed quantitative changes in  $\beta$ -sheet are complying well with qualitative changes. A maximum decrease of 32% was observed until  $0.06 \text{ mmol L}^{-1}$  (just above  $C_1$ ) in the aggregation regime. Beyond  $0.06 \text{ mmol L}^{-1}$  gain in  $\beta$ -sheet content was observed until the post-vesicular regime. An overall 16% decrease in  $\beta$ -sheet sheet content was observed until 0.58

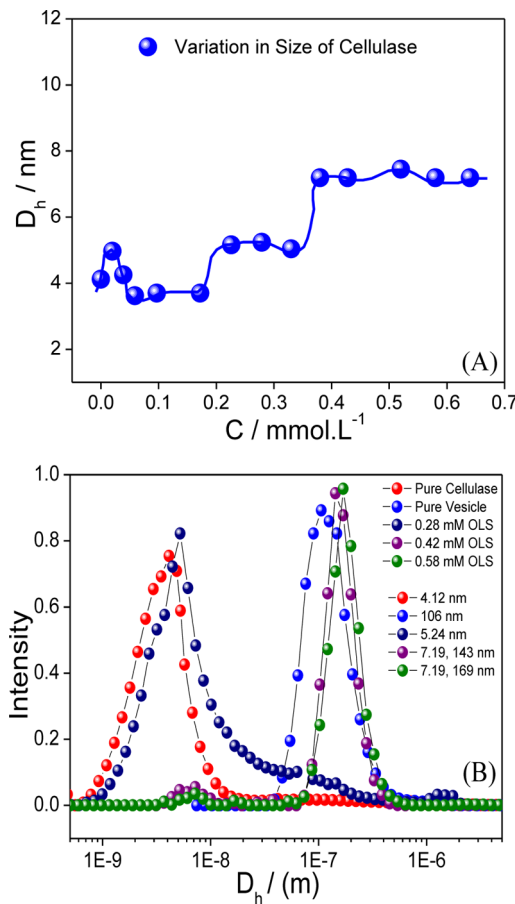


**Figure 5.** (A) Variation in the hydrodynamic diameter ( $D_h$ ) of cellulase as a function of  $[C_8\text{mim}][C_{12}\text{OSO}_3]$  concentration. (B) CONTIN plots of native cellulase and cellulase +  $[C_8\text{mim}][C_{12}\text{OSO}_3]$  at different concentrations.

mmol L<sup>-1</sup> in the post-vesicular regime. The initial decrease in the monomeric binding is mainly due to the binding of  $[C_8\text{mim}]^+$  to the negatively charged (Asp, Glu) and  $[C_{12}\text{OSO}_3]^-$  to the positively charged (Lys, Arg) aa at the surface of cellulase. More sites for  $[C_8\text{mim}]^+$  binding have been demonstrated from the binding isotherms wherein a higher  $dH$  was found to release upon  $[C_8\text{mim}]^+$  binding to cellulase in the monomeric regime. Moreover, the decrease in  $\beta$ -sheet in this regime has also been reflected in the tertiary structure due to the disturbance of disulfide bonds which maintains the tertiary structure. Increase in  $\beta$ -sheet in the aggregation region is due to simultaneous cross-linking of  $[C_8\text{mim}][C_{12}\text{OSO}_3]$  with the charged and hydrophobic aa residues. The decrease in  $\beta$ -sheet from sub-aggregation to the vesicular regimes is due to the cooperative binding (consequent electrostatic and hydrophobic interactions) in the middle part of the enzyme having maximum concentration of charged and hydrophobic residues. Regain and constancy of  $\beta$ -sheet in the post-vesicular regime is due to the fact that  $[C_8\text{mim}][C_{12}\text{OSO}_3]$  self-associations predominate the  $[C_8\text{mim}][C_{12}\text{OSO}_3]$ –cellulase interactions.

**3.2.3. Alteration in the Hydrodynamic Diameter.**  $[C_8\text{mim}][C_{12}\text{OSO}_3]$  induced alterations in the size of cellulase have been detected through dynamic light scattering analysis. The size of cellulase can change either due to unfolding/refolding upon  $[C_8\text{mim}][C_{12}\text{OSO}_3]$  interaction or complexation of  $[C_8\text{mim}][C_{12}\text{OSO}_3]$  with cellulase.  $[C_8\text{mim}][C_{12}\text{OSO}_3]$  induced alterations in the hydrodynamic diameter

( $D_h$ ) of cellulase are shown in Figure 5A, and corresponding CONTIN plots are shown in Figure S9 (Supporting Information). Native cellulase has a  $D_h$  of 4.12 nm.  $D_h$  increased initially up to 0.019 mmol L<sup>-1</sup> (just below  $C_1$ ) due to unfolding of cellulase. Beyond 0.019 mmol L<sup>-1</sup>,  $D_h$  decreased to 3.62 nm until 0.060 mmol L<sup>-1</sup> and remained constant at 3.7 nm until 0.17 mmol L<sup>-1</sup> due to refolding of the cellulase. Above 0.17 mmol L<sup>-1</sup>,  $D_h$  increased to 5.16 nm and remained almost constant until 0.33 mmol L<sup>-1</sup>.  $D_h$  increased again in the vesicular regime to 7.19 nm and remained constant thereafter in the post-vesicular regime, indicating the stabilization of cellulase in this conformation in a pool of vesicles. The DLS results are validating the fluorescence and CD observations that cellulase undergoes consequent folding/refolding upon  $[C_8\text{mim}][C_{12}\text{OSO}_3]$  binding in various concentration regimes. It has also been observed that the peak intensity of cellulase decreased to a considerable extent in the vesicular and post-vesicular regimes and the size of  $[C_8\text{mim}][C_{12}\text{OSO}_3]$  vesicles (106 nm) increased from 140 nm at 0.33 mmol L<sup>-1</sup> (vesicular regime) to 200 nm until 0.64 mmol L<sup>-1</sup> (post-vesicular regime) in the presence of cellulase (Figure S6B and Figure S9, Supporting Information). These observations are citing the fact that cellulase gets adsorbed either at the surface or in the bilayer of vesicles, hence causing the swelling of vesicles.

**3.3. Functional Stability of Cellulase in Various Concentration Regimes of Cellulase– $[C_8\text{mim}][C_{12}\text{OSO}_3]$  Interaction.** The functional stability of cellulase at different concentrations of  $[C_8\text{mim}][C_{12}\text{OSO}_3]$  has been checked through the DNS sugar assay test.<sup>52</sup> The activity vs concentration profiles are shown in Figure 6. Sugar impurities in the purchased enzymes have been checked by doing the DNS analysis in the absence of CMC. Nonappearance of dark brown color (bottle 1 of image, Figure 6) demonstrated the absence of sugar impurities. Appearance of dark brown color

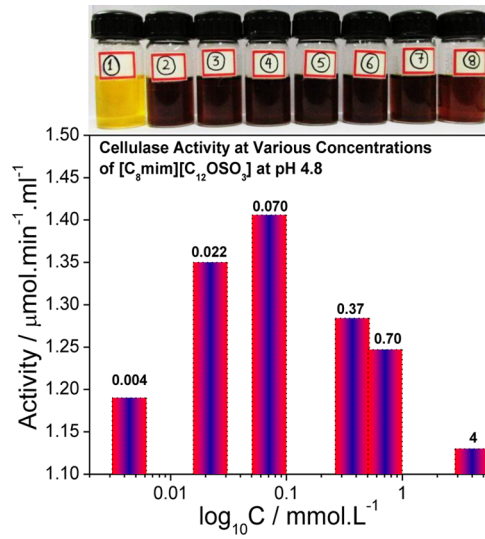
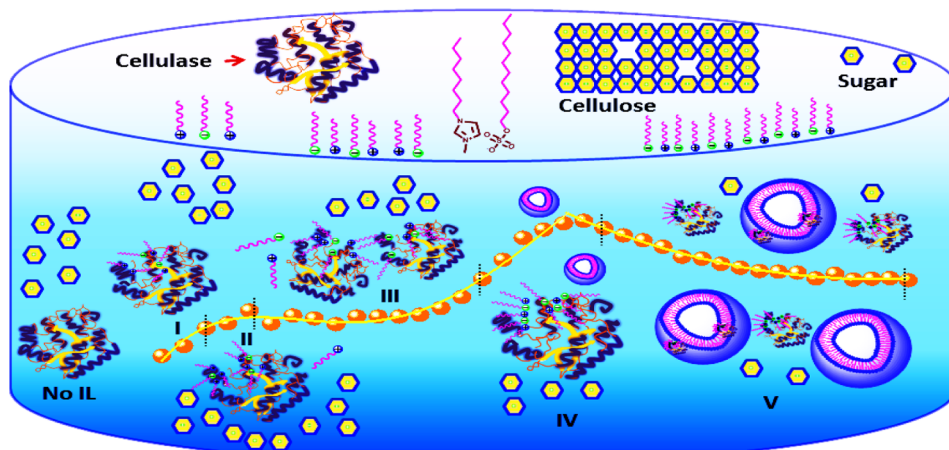


**Figure 6.** Cellulase activity in different concentration regimes of cellulase– $[C_8\text{mim}][C_{12}\text{OSO}_3]$  interaction. The numbers over the pillars signify the concentration (mmol L<sup>-1</sup>) of the  $[C_8\text{mim}][C_{12}\text{OSO}_3]$ . The image at the top of the figure indicates the color developed due to reduction of DNS by sugar released by hydrolysis of carboxymethylcellulose (CMC) by cellulase at different concentrations of  $[C_8\text{mim}][C_{12}\text{OSO}_3]$ . 1 = no CMC. 2–7 = at  $[C_8\text{mim}][C_{12}\text{OSO}_3]$  concentrations (mmol L<sup>-1</sup>) of 0.004, 0.022, 0.071, 0.37, 0.7, and 4. 8 = no  $[C_8\text{mim}][C_{12}\text{OSO}_3]$ .

**Scheme 2. Structural Alterations and Functional Activity of Cellulase in Various Concentration Regimes (I–V) of  $[C_8\text{mim}][C_{12}\text{OSO}_3]$ –Cellulase Interaction<sup>a</sup>**



<sup>a</sup>No IL signifies native enzyme, cellulase activity (CA) = 1.32 unit/mg, I → monomeric regime, slight unfolding, CA = 1.35 unit/mg, II → cellulase induced aggregation regime, unfolding followed by refolding, CA = 1.41 unit/mg, III → shared aggregation regime, unfolding due to sharing of aggregates by two or more cellulases, CA = 1.28 unit/mg, IV → aggregation regime, unfolding CA = 1.24 unit, V → post-aggregation regime, cellulase conformational stability, CA = 1.13 unit. The yellow hexagon shape signifies sugar released upon cellulose hydrolysis. Overall activity, >1 unit/mg signifying the functional activity of cellulase at all concentrations of  $[C_8\text{mim}][C_{12}\text{OSO}_3]$ .

(bottles 2–8 of image, Figure 6) at different concentrations of  $[C_8\text{mim}][C_{12}\text{OSO}_3]$  in the presence of CMC and cellulase has indicated that cellulase is active in the presence of  $[C_8\text{mim}][C_{12}\text{OSO}_3]$ . The calculated activity of the enzyme in the absence of  $[C_8\text{mim}][C_{12}\text{OSO}_3]$  at pH 4.8 has been found to be 1.32 unit/mg, which is complying with the Sigma-Aldrich value of ≥1 unit/mg. The cellulase activity remained >1 in all the concentration regimes. The highest activity of 1.4 unit/mg (>1.32 unit/mg for pure enzyme) was found at 0.07 mmol L<sup>-1</sup> in the aggregation regime wherein a loss in tertiary and secondary structure was observed from fluorescence and CD measurements. The Asp and Glu found in the catalytic domain of cellulase are known to catalyze the hydrolysis of cellulose by disrupting the glycosidic linkage. Thus, the slight unfolding of cellulase might have exposed Asp and Glu residues in the catalytic domains which drive the higher sugar conversion in this regime. Although there is a decrease in activity in the vesicular and post-vesicular regimes, the value is always >1 unit/mg, citing the significant functional stability of cellulase in these regimes. Nonionic surfactants and mixed micelles of ionic surfactants have been reported in the literature to maintain the activity of cellulase in detergents due to the decrease in ionic interactions with the enzymes.<sup>53,54</sup> Reduction in CVC of  $[C_8\text{mim}][C_{12}\text{OSO}_3]$  to 0.35 mmol L<sup>-1</sup> compared to its individual ionic moieties has a significant contribution to the decrease in ionic interactions, thus leading to functional stability of cellulase in  $[C_8\text{mim}][C_{12}\text{OSO}_3]$  solution. The mechanism of alteration in the structure and functional stability of cellulase in different concentration regimes of  $[C_8\text{mim}][C_{12}\text{OSO}_3]$ –cellulase interaction is depicted in Scheme 2.

#### 4. CONCLUSION

Inferences obtained from the comparative technical analysis of  $[C_8\text{mim}][C_{12}\text{OSO}_3]$  interaction with cellulase at pH 4.8 have led us to conclude the present work based on the following points: (1)  $[C_8\text{mim}][C_{12}\text{OSO}_3]$  binds sequentially to cellulase from the monomeric to vesicular regime wherein electrostatic interactions are reinforced by hydrophobic interactions. (2)

Cellulase has more binding sites for  $[C_8\text{mim}]^+$  as compared to  $[C_{12}\text{OSO}_3]^-$ , evidenced by the higher contribution to the overall enthalpy change ( $-1.32 \text{ kJ mol}^{-1}$ ) by the  $[C_8\text{mim}][\text{Cl}]$ –cellulase system ( $-0.9 \text{ kJ mol}^{-1}$ ) than the SDS–cellulase system ( $-0.42 \text{ kJ mol}^{-1}$ ). (3) Structurally,  $[C_8\text{mim}][C_{12}\text{OSO}_3]$  unfolds cellulase mainly in the monomeric binding regime evidenced by a decrease in  $I_{\text{flr}}$ ,  $\beta$ -sheet content, and  $-\theta_{217 \text{ nm}}$  CD peak and an increase in the  $D_h$  of cellulase, refolds in the aggregation regime, again unfolds in the shared aggregation regime, and stabilizes the transition conformation in the post-vesicular regime. However, the overall conformational change is not very high, as evidenced by a decrease in  $I_{\text{flr}}$  by just 4.3%,  $\beta$ -sheet content from 57.5 to 48.2%, and increase in  $D_h$  from 4.12 to 7.16 nm from native cellulase to cellulase in the presence of ~0.6 mmol L<sup>-1</sup> of  $[C_8\text{mim}][C_{12}\text{OSO}_3]$  in the post-vesicular regime. (4) Functionally, cellulase has been found to be active in all the concentration regimes with an activity of >1 unit/mg. The activity was highest in the aggregation concentration regime which may be due to exposure of more catalytically active Glu and Asp aa due to cellulase unfolding in this regime. (5) A low value of  $\Delta G^\circ_S = -6.7 \text{ kJ mol}^{-1}$  indicated a lower feasibility of  $[C_8\text{mim}][C_{12}\text{OSO}_3]$  interaction with cellulase as compared to the self-association of  $[C_8\text{mim}][C_{12}\text{OSO}_3]$ . Considering the inferences obtained from the technical analysis, we conclude that  $[C_8\text{mim}][C_{12}\text{OSO}_3]$  is a potential alternative for mixed micelles and nonionic surfactants for cellulase stabilization in detergent industries.

#### ASSOCIATED CONTENT

##### S Supporting Information

Annexure S1 showing how several parameters were calculated and Figures S1–S9 showing differential power plots, binding isotherms, UV spectra, fluorescence spectra, concentration vs wavelength variation plot, fluorescence emission spectra and corresponding intensity variation profiles, plot showing variation in  $\beta$ -sheet content as a function of concentration, and CONTIN plots. This material is available free of charge via the Internet at <http://pubs.acs.org>.

## AUTHOR INFORMATION

### Corresponding Author

\*E-mail: mailme\_arvind@yahoo.com; arvind@csmcri.org. Phone: +91-278-2567039. Fax: +91-278-2567562.

### Notes

The authors declare no competing financial interest.

## ACKNOWLEDGMENTS

The authors are thankful to Department of Science and Technology (DST), Government of India, for financial support for this work (No. SB/S1/PC-104/2012). The analytical division of CSMCRI is acknowledged for sample characterization. The authors are thankful to Mr. K. Srinivasa Rao and Dr. Tushar J Trivedi for assisting in synthesis of  $[C_8\text{mim}]$   $[C_{12}\text{OSO}_3]$ .

## REFERENCES

- (1) Rogers, R. D.; Seddon, K. R.; Volkov, S. *Green Industrial Applications of Ionic Liquids*; NATO Science Series; Kluwer: Dordrecht, The Netherlands, 2002.
- (2) Bowers, J.; Butts, P.; Martin, J.; Vergara-Gutierrez, C.; Heenan, K. Aggregation Behavior of Aqueous Solution of Ionic Liquids. *Langmuir* **2004**, *20*, 2191–2198.
- (3) Thomaier, S.; Kunz, W. Aggregates in mixtures of ionic liquids. *J. Mol. Liq.* **2007**, *130*, 104–107.
- (4) Wang, H. Y.; Wang, J. J.; Zhang, S. B.; Xuan, X. P. Structural Effects of Anion and Cation on the Aggregation Behavior of Ionic Liquids in Aqueous Solution. *J. Phys. Chem. B* **2008**, *112*, 16682–16689.
- (5) Zhao, Y.; Gao, S. J.; Wang, J. J.; Tang, J. M. Aggregation of Ionic Liquids  $[C_n\text{mim}][\text{Br}]$  ( $n = 4, 6, 8, 10, 12$ ) in  $\text{D}_2\text{O}$ : A NMR Study. *J. Phys. Chem. B* **2008**, *112*, 2031–2039.
- (6) Ao, M.; Xu, G.; Zhu, Y.; Bai, Y. Synthesis and Properties of Ionic Liquid-type Gemini Imidazolium Surfactants. *J. Colloid Interface Sci.* **2008**, *326*, 490–495.
- (7) Preiss, U.; Jungnickel, C.; Thoming, J.; Krossing, I.; Luczak, J.; Diedenhofen, M.; Klamt, A. Predicting the Critical Micelle Concentrations of Aqueous Solutions of Ionic Liquids and Other Ionic Surfactants. *Chem.—Eur. J.* **2009**, *15*, 8880–8885.
- (8) Ao, M.; Xu, G.; Pang, J.; Zhao, T. Comparison of Aggregation Behaviors between Ionic Liquid-Type Imidazolium Gemini Surfactant  $[C_{12}\text{-}4\text{-}C_{12}\text{im}] \text{Br}_2$  and Its Monomer  $[C_{12}\text{mim}] \text{Br}$  on Silicon Wafer. *Langmuir* **2009**, *25*, 9721–9727.
- (9) Chamiot, B.; Rizzi, C.; Gaillon, L.; Sirieix-Plenet, J.; Lelievre, J. Redox-Switched Amphiphilic Ionic Liquid Behavior in Aqueous Solution. *Langmuir* **2009**, *25*, 1311–1315.
- (10) Li, X.; Gao, Y.; Liu, J.; Zheng, L.; Chen, B.; Wub, L.; Tung, C. Aggregation behavior of a chiral long-chain ionic liquid in aqueous solution. *J. Colloid Interface Sci.* **2010**, *343*, 94–101.
- (11) Singh, T.; Drechsler, M.; Müller, A. H. E.; Mukhopadhyay, I.; Kumar, A. Micellar Transitions in the Aqueous Solutions of a Surfactant Like Ionic Liquid. 1-Butyl-3-methylimidazolium octylsulfate. *Phys. Chem. Chem. Phys.* **2010**, *12*, 11728–11735.
- (12) Bhadani, A.; Singh, S. Synthesis and Properties of Thioether Spacer Containing Gemini Imidazolium Surfactants. *Langmuir* **2011**, *27*, 14033–14044.
- (13) Trivedi, T. J.; Rao, K. S.; Singh, T.; Mandal, S. K.; Sutradhar, N.; Panda, A. B.; Kumar, A. Task-Specific, Biodegradable Amino Acid Ionic Liquid Surfactants. *ChemSusChem* **2011**, *4*, 604–608.
- (14) Rao, K. S.; Singh, T.; Trivedi, T. J.; Kumar, A. Aggregation Behavior of Amino Acid Ionic Liquid Surfactants in Aqueous Media. *J. Phys. Chem. B* **2011**, *115*, 13847–13853.
- (15) Rao, K. S.; Trivedi, T. J.; Kumar, A. Aqueous Biamphiphilic Ionic Liquid System: Self Assembly and synthesis of gold nanocrystals/nanoplates. *J. Phys. Chem. B* **2012**, *116*, 14363–14374.
- (16) Jiao, J.; Dong, B.; Zhang, H.; Zhao, Y.; Wang, X.; Wang, R.; Yu, L. Aggregation Behaviors of Dodecyl Sulfate-Based Anionic Surface Active Ionic Liquids in Water. *J. Phys. Chem. B* **2012**, *116*, 958–965.
- (17) Jingjing, J.; Bing, H.; Meijia, L.; Ni, C.; Li, Y.; Min, L. Salt-free catanionic Surface Active Ionic Liquids 1-alkyl-3-methylimidazolium alkylsulfate: Aggregation Behavior in Aqueous Solution. *J. Colloid Interface Sci.* **2013**, *412*, 24–30.
- (18) Lingling, Ge.; Qi, W.; Duo, W.; Xiaohong, Z.; Rong, G. Aggregation of Double-Tailed Ionic Liquid 1,3-Dioctylimidazolium Bromide and the Interaction with Triblock Copolymer F127. *J. Phys. Chem. B* **2013**, *117*, 15014–15022.
- (19) Teresa, G. M.; Isabel, R.; Lourdes, P.; Angeles, M.; Francesc, C. Aggregation Behavior and Antimicrobial Activity of Ester-Functionalized Imidazolium- and Pyridinium-Based Ionic Liquids in Aqueous Solution. *Langmuir* **2013**, *29*, 2536–2545.
- (20) Cheng, N.; Yu, P.; Wang, T.; Sheng, X.; Bi, Y.; Gong, Y.; Yu, L. Self-Aggregation of New Alkylcarboxylate-Based Anionic Surface Active Ionic Liquids: Experimental and Theoretical Investigations. *J. Phys. Chem. B* **2014**, *118*, 2758–2768.
- (21) Wei, Y.; Wang, F.; Zhang, Z.; Ren, C.; Lin, Y. Micellization and Thermodynamic Study of 1-Alkyl-3-methylimidazolium Tetrafluoroborate Ionic Liquids in Aqueous Solution. *J. Chem. Eng. Data* **2014**, *59*, 1120–1129.
- (22) Rao, K. S.; Gehlot, P. S.; Trivedi, T. J.; Kumar, A. Self-assembly of AOT Derived Anionic Surface Active ILs in Aqueous Media. *J. Colloid Interface Sci.* **2014**, *428*, 267–275.
- (23) Ananthapadmanabhan, K. P. In *Interactions of Surfactants with Polymers and Proteins*; Goddard, E. D., Ananthapadmanabhan, K. P., Eds.; CRC Press, Inc: London, U.K., 1993; Chapter 8.
- (24) Jones, M. N. Surfactant Interactions with Biomembranes and Proteins. *Chem. Soc. Rev.* **1992**, *21*, 127–136.
- (25) Dalgleish, D. G. In *Emulsions and Emulsion Stability*; Sjöblom, J., Ed.; Marcel Dekker: New York, 1996; Chapter 5.
- (26) Geng, F.; Zheng, L.; Liu, J.; Yu, L.; Tung, C. Interactions between a Surface Active Imidazolium Ionic Liquid and BSA. *Colloid Polym. Sci.* **2009**, *287*, 1253–1259.
- (27) Geng, F.; Zheng, L.; Yu, L.; Li, G.; Tung, C. Interaction of Bovine Serum Albumin and Long-Chain Imidazolium Ionic Liquid Measured by Fluorescence Spectra and Surface Tension. *Process Biochem.* **2010**, *45*, 306–311.
- (28) Singh, T.; Boral, S.; Bohidar, H. B.; Kumar, A. Interaction of Gelatin with Room Temperature Ionic Liquids: A Detailed Physicochemical Study. *J. Phys. Chem. B* **2010**, *114*, 8441–8448.
- (29) Singh, T.; Bharmoria, P.; Morikawa, M.; Kimizuka, N.; Kumar, A. Ionic Liquids Induced Structural Changes of Bovine Serum Albumin in Aqueous Media: A Detailed Physicochemical and Spectroscopic Study. *J. Phys. Chem. B* **2012**, *116*, 11924–11935.
- (30) Bharmoria, P.; Rao, K. S.; Trivedi, T. J.; Kumar, A. Biamphiphilic Ionic Liquid Induced Folding Alterations in the Structure of Bovine Serum Albumin in Aqueous Medium. *J. Phys. Chem. B* **2014**, *118*, 115–124.
- (31) Wang, X.; Liu, J.; Sun, L.; Yu, L.; Jiao, J.; Wang, R. Interaction of Bovine Serum Albumin with Ester-Functionalized Anionic Surface-Active Ionic Liquids in Aqueous Solution: A Detailed Physicochemical and Conformational Study. *J. Phys. Chem. B* **2012**, *116*, 12479–12488.
- (32) Yan, H.; Wu, J.; Dai, G.; Zhong, A.; Chen, H.; Yang, J.; Han, D. Interaction Mechanism of Ionic Liquids  $[C_n\text{mim}][\text{Br}]$  ( $n = 4, 6, 8, 10$ ) with Bovine Serum Albumin. *J. Lumin.* **2012**, *132*, 622–628.
- (33) Pinto, P. C. A. G.; Ribeiro, D. M. G. P.; Azevedo, A. M. O.; Justina, V. D.; Cunha, E.; Bica, K.; Vasiloiu, M.; Reisa, S.; Saraiva, M. L. M. F. S. Active Pharmaceutical Ingredients Based on Salicylate Ionic Liquids: Insights Into the Evaluation of Pharmaceutical Profiles. *New J. Chem.* **2013**, *37*, 4095–4102.
- (34) Kumar, P. B.; Aniruddha, G.; Nikhil, G. Deciphering the Interaction of a Model Transport Protein with a Prototypical Imidazolium Room Temperature Ionic Liquid: Effect on the Conformation and Activity of the Protein. *J. Photochem. Photobiol. B* **2014**, *133*, 99–107.

- (35) Otzen, D. Protein-Surfactant Interactions: A Tale of Many States. *Biochim. Biophys. Acta* **2011**, *1814*, 562–591.
- (36) Penttilä, M.; Lehtovaara, P.; Nevalainen, H.; Bhikhabhai, R.; Knowles, J. Homology Between Cellulase Genes of *Trichoderma reesei*: Complete Nucleotide Sequence of the Endoglucanase I Gene. *Gene* **1986**, *45*, 253–263.
- (37) Ohmiya, K.; Sakka, K.; Karita, S.; Kimura, T. Structure of Cellulases and their Applications. *Biotechnol. Genet. Eng. Rev.* **1997**, *14*, 365–414.
- (38) Xiang, J.; Fan, J.; Chen, N.; Chen, J.; Liang, Y. Interaction of Cellulase with Sodium Dodecylsulfate at Critical Micelle Concentration Level. *Colloids Surf., B* **2006**, *49*, 175–180.
- (39) Rastegari, A. A.; Bordbarb, A.; Taheri-Kafranib, A. C cationic surfactants: Using Surfactant Membrane Selective Electrodes and Fluorescence Spectroscopy. *Colloids Surf., B* **2009**, *73*, 132–139.
- (40) Eriksson, T.; Börjesson, J.; Tjerneld, F. Mechanism of Surfactant Effect in Enzymatic Hydrolysis of Lignocellulose. *Enzyme Microb. Technol.* **2002**, *31*, 353–364.
- (41) Lu, R.; Cao, A.; Lai, L.; Zhu, B.; Zhao, G.; Xiao, J. Interaction Between Bovine Serum Albumin and Equimolarly Mixed Cationic-Anionic Surfactants Decyltriethylammonium bromide-Sodium decylsulfonate. *Colloids Surf., B* **2005**, *41*, 139–143.
- (42) Stoner, M. R.; Dale, D. A.; Gualfetti, P. J.; Becker, T.; Randolph, T. W. Surfactant-Induced Unfolding of Cellulase: Kinetic Studies. *Biotechnol. Prog.* **2006**, *22*, 225–232.
- (43) Pucci, C.; Scipioni, A.; Mesa, C. L. Albumin Binding onto Synthetic Vesicles. *Soft Matter* **2012**, *8*, 9669–9675.
- (44) Sciscione, F.; Pucci, C.; Mesa, C. L. Binding of a Protein or a Small Polyelectrolyte onto Synthetic Vesicles. *Langmuir* **2014**, *30*, 2810–2819.
- (45) Bharmoria, P.; Kumar, A. Interactional Behaviour of Surface Active Ionic Liquids with Gelling Biopolymer Agarose in Aqueous Medium. *RSC Adv.* **2013**, *3*, 19600–19608.
- (46) Tama, K. C.; Wyn-Jones, E. Insights on Polymer Surfactant Complex Structures During the Binding of Surfactants to Polymers as Measured by Equilibrium and Structural Techniques. *Chem. Soc. Rev.* **2006**, *35*, 693–709.
- (47) Jones, M. N.; Skinner, H. A.; Tipping, E.; Wilkinson, A. The interaction Between Ribonuclease A and Surfactants. *Biochem. J.* **1973**, *135*, 231–236.
- (48) Brown, J. R. Structure of Bovine Serum Albumin. *Fed. Proc.* **1975**, *34*, 591–591.
- (49) Schmid, F. X. Optical Spectroscopy to Characterize Protein Conformation. In *Protein Structure: A Practical Approach*; Creighton, T. E., Ed.; IRL Press: Oxford, U.K., 1997; pp 261–298.
- (50) Markus, G.; Love, R. L.; Wissler, F. C. Mechanism of Protection by Anionic Detergents against Denaturation of Serum Albumin. *J. Biol. Chem.* **1964**, *239*, 3687–3693.
- (51) Deep, S.; Ahluwalia, J. C. Interaction of Bovine Serum Albumin with Anionic Surfactant. *Phys. Chem. Chem. Phys.* **2001**, *3*, 4583–4591.
- (52) Iqbal, H. M. N.; Ahmed1, I.; Zia, M. A.; Irfan, M. Purification and Characterization of the Kinetic Parameters of Cellulase Produced from Wheat Straw by *Trichoderma viride* under SSF and its Detergent Compatibility. *Adv. Biosci. Biotechnol.* **2011**, *2*, 149–156.
- (53) Bajpai, D.; Tyagi, V. K. Laundry Detergents: an Overview. *J. Oleo Sci.* **2007**, *56*, 327–340.
- (54) Sehgal, P.; Mogensen, J. E.; Otzen, D. E. Using Micellar Mole Fractions to Assess Membrane Protein Stability in Mixed Micelles. *Biochim. Biophys. Acta* **2005**, *1716*, 59–68.